intraperitoneal injection 1, 4, and 14 days after surgery. The concentration of anti–IL-10 receptor antibody was chosen based on the previous study of its efficacy.[12] Four weeks after surgery, echocardiographic and hemodynamic measurements were performed. Separate groups of mice were used in the MI+αGC group in experiment 2.

Experiment 4: Specificity of αGC for NKT Cells

Vα14$^+$ NKT cell-deficient Jα18$^{-/-}$ (Jα18 KO) mice were provided by Dr M. Taniguchi (RIKEN, Yokohama, Japan) and back-crossed 10 times to C57BL/6J.[17] Sham and MI mice were created in male Jα18 KO mice as described in experiment 1. Each group of mice was treated identically to experiment 2. Thus, the experiment was performed in the following 4 groups; KO+sham+PBS, KO+sham+αGC, KO+MI+PBS, and KO+MI+αGC. One week after surgery, all mice (n=9 for each group) were euthanized and used for immunohistochemistry (n=3 for each group) and for qRT-PCR (n=6 for each group). These analyses were performed as described in experiment 2.

Statistical Analysis

Data are expressed as mean±SEM. Survival analysis was performed by the Kaplan-Meier method, and between-group differences in survival were tested by the log-rank test. A between-group comparison of means was performed by 1-way ANOVA, followed by *t* test. The Bonferroni correction was applied for multiple comparisons of means. $P<0.05$ was considered statistically significant.

The authors had full access to and take full responsibility for the integrity of the data. All authors had read and agreed to the manuscript as written.

Results

Experiment 1: Time-Dependent Changes of iNKT Cell Receptors in Post-MI Hearts

The quantification of iNKT cells by Vα14/Jα18 gene expression demonstrated that iNKT cell infiltration into the noninfarcted LV was significantly enhanced at 7 days (1.7±0.2-fold changes from baseline, $P<0.05$ versus baseline) after MI and returned to baseline at 14 and 28 days after MI (1.0±0.2- and 1.1±0.1-fold changes from baseline, respectively). In the infarcted LV, its gene expression was significantly elevated 7 days and remained elevated 28 days after MI (data not shown).

Experiment 2: Effects of iNKT Cell Activation on Post-MI Hearts

By using flow cytometric analysis, iNKT cells were detected in LV from all groups of mice (Figure 1A). αGC injection increased iNKT cells infiltration into the noninfarcted LV both in sham+αGC and MI+αGC mice after 7 days (Figure 1A). Moreover, it remained enhanced at 28 days in MI+αGC (Figure 1A).

Quantitative RT-PCR also demonstrated that gene expression of Vα14/Jα18, a marker of iNKT cell infiltration, was significantly elevated in the noninfarcted LV from sham+αGC and MI+αGC mice after 7 days (Figure 1B). Interestingly, it remained significantly increased at 28 days only in MI+αGC (Figure 1B).

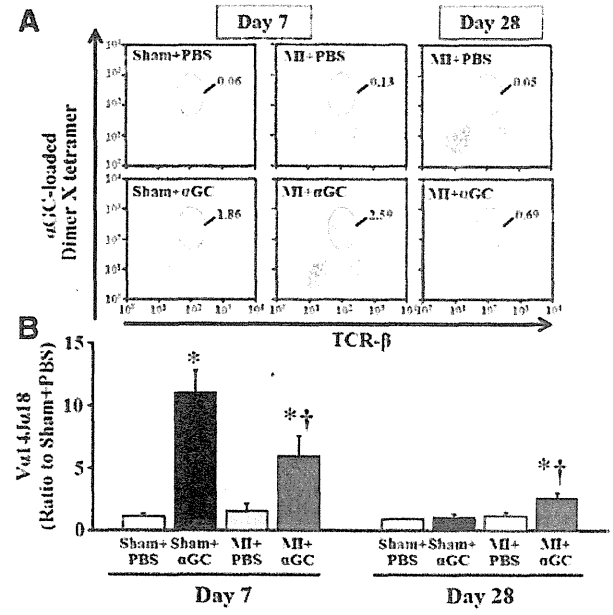

Figure 1. A, Representative flow cytometric assessment of cardiac mononuclear cells obtained from sham+PBS, sham+αGC, MI+PBS, and MI+αGC at days 7 and 28. Cardiac mononuclear cells from 5 different mice for each group were pooled and analyzed. The experiments were performed 3 times. iNKT cells were gated as the αGC-loaded dimer X tetramer$^+$TCR-β$^+$ population. The **inset** numbers are a percentage of the gated region of the samples. **B**, Gene expression of Vα14/Jα18 in noninfarcted LV from sham+PBS, sham+αGC, MI+PBS, and MI+αGC 7 days (n=6) and 28 days (n=4) after surgery. They were normalized to GAPDH gene expression and expressed as ratio to sham+PBS values. Data are expressed as mean±SEM. *$P<0.05$ versus sham+PBS, †$P<0.05$ versus MI+PBS.

Survival

There were no deaths in sham-operated groups. The survival rate during 28 days was significantly higher in MI+αGC compared with MI+PBS mice (59% versus 32%; $P<0.05$; Figure 2A). Thirteen MI+PBS (42%) and 8 MI+αGC (30%) mice died of LV rupture (P=NS).

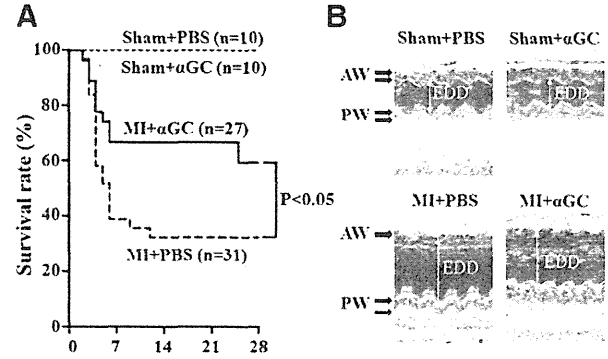

Figure 2. A, Percent survival of sham+PBS (n=10), sham+αGC (n=10), MI+PBS (n=31), and MI+αGC (n=27) mice shown by Kaplan-Meier method. B, Representative M-mode echocardiographic images obtained from sham+PBS, sham+αGC, MI+PBS, and MI+αGC. AW indicates anterior wall; PW, posterior wall; EDD, end-diastolic diameter.

Table 1. Echocardiography, Hemodynamics, and Organ Weights in Experiment 2

	Sham+PBS (n=10)	Sham+αGC (n=10)	MI+PBS (n=10)	MI+αGC (n=16)
Echocardiography				
Heart rate, bpm	522±10	522±12	531±16	520±13
LVEDD, mm	3.4±0.1	3.4±0.04	5.4±0.1*	5.0±0.1*†
LVESD, mm	2.1±0.03	2.1±0.04	4.5±0.1*	4.1±0.1*†
FS, %	38.2±0.7	38.3±0.6	16.5±0.6*	18.8±0.6*†
AWT, mm	0.63±0.01	0.62±0.01	0.31±0.01*	0.30±0.01*
PWT, mm	0.68±0.02	0.68±0.01	0.97±0.01*	0.96±0.02*
Hemodynamics				
Heart rate, min	507±9	499±9	485±23	495±11
Mean AoP, mm Hg	78.1±2	77.7±2	75.0±3	79.3±1
LVEDP, mm Hg	1.7±0.3	2.3±0.1	10.7±1.1*	6.6±0.6*†
LV +dP/dt, mm Hg/s	15 625±623	14 972±398	7352±697*	9386±476*†
LV –dP/dt, mm Hg/s	9983±697	9130±691	5045±482*	5861±286*
Organ weights				
Body wt, g	25.1±0.3	24.9±0.2	24.5±0.4	24.8±0.3
Heart wt/body wt, mg/g	4.6±0.1	4.5±0.1	6.8±0.2*	6.1±0.1*†
Lung wt/body wt, mg/g	5.2±0.03	5.2±0.1	7.2±0.7*	5.9±0.2†
Infarct size, %	...	...	56±2	55±1

LVEDD indicates left ventricular end-diastolic diameter; LVESD, left ventricular end-systolic diameter; FS, fractional shortening; AWT, anterior wall thickness; PWT, posterior wall thickness; AoP, aortic pressure; LVEDP, left ventricular end-diastolic pressure; wt, weight. Data are mean±SEM.

*P<0.05 versus sham+PBS.

†P<0.05 versus MI+PBS.

Echocardiography and Hemodynamics

The echocardiographic and hemodynamic data from 4 groups of survived mice at 28 days are shown in Figure 2B and Table 1. There were no significant differences in either echocardiographic or hemodynamic parameters between sham+PBS and sham+αGC mice. LV diameters were significantly greater and LV fractional shortening was significantly lower in MI mice than sham mice. These changes were ameliorated by the treatment of MI mice with αGC. There were no significant differences in heart rate or aortic blood pressure among groups. LV end-diastolic pressure (LVEDP) was significantly increased, and LV +dP/dt and LV –dP/dt were significantly decreased in MI compared with sham, which was ameliorated by the treatment of MI mice with αGC.

Organ Weights, Infarct Size, and Histology

There were no significant differences in heart weight/body weight and lung weight/body weight between sham+PBS and sham+αGC mice (Table 1). In agreement with LVEDP, heart weight/body weight and lung weight/body weight were increased in MI mice, and these increases were significantly attenuated in MI+αGC (Table 1).

Infarct size measured by the morphometric analysis was comparable (56±2% versus 55±1%; P=NS) between MI+PBS (n=6) and MI+αGC (n=6) groups (Table 1).

Histomorphometric analysis of noninfarcted LV sections showed that myocyte cross-sectional area was increased in MI+PBS compared with sham mice and was significantly attenuated in MI+αGC (Figure 3A). Collagen volume fraction was also increased in MI+PBS compared with sham mice and was significantly attenuated in MI+αGC (Figure 3A).

There were rare TUNEL-positive nuclei in both sham and sham+αGC mice. The number of TUNEL-positive myocytes in the noninfarcted LV was increased in MI+PBS and was significantly decreased in MI+αGC (Figure 3B).

Myocardial MMP Activity

Representative gelatin zymography of the noninfarcted LV tissue at day 7 from 4 groups of mice was shown in Figure 4A. There were no zymographic MMP-2 and 9 levels in the sham+PBS and sham+αGC. Zymographic MMP-2 level was significantly increased in MI+PBS mice compared with sham mice at day 7. αGC injection significantly decreased this after MI (Figure 4B). Zymographic MMP-9 level was also increased in MI+PBS mice compared with sham mice at day 7, which, however, was not affected by αGC (Figure 4C).

Zymographic MMP-2 level was increased in MI+PBS mice also at day 28, and αGC injection tended to decrease it (3.7±1.1 versus 2.1±0.8 in ratio to sham, P=0.08).

Inflammatory and Cytokine Gene Expression

Immunohistochemical stainings for MAC3 and CD3 were increased in MI+PBS compared with sham+PBS and were further increased by αGC at day 7 (Figure 5). MPO-positive cells were not detected in the LV tissue from either group of mice (data not shown).

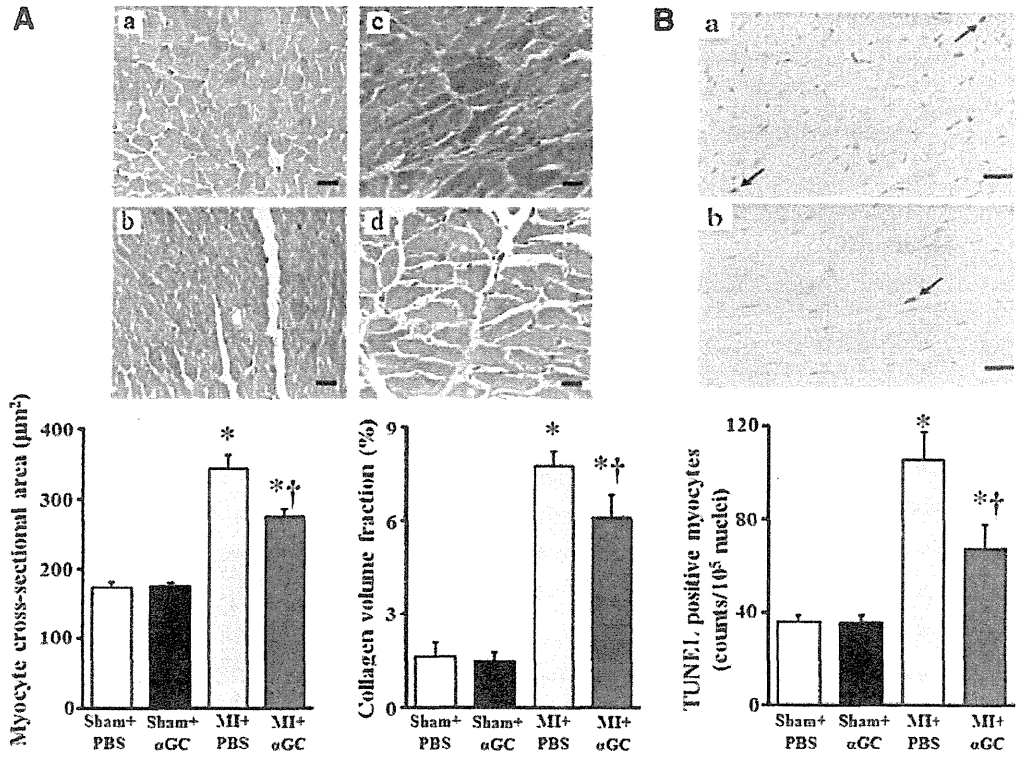

Figure 3. A, Representative high-power photomicrographs of LV cross sections stained with Masson trichrome from sham+PBS (a), sham+αGC (b), MI+PBS (c), and MI+αGC (d) and summary data of myocyte cross-sectional area and collagen volume fraction in 4 groups of mice (n=6). Scale bar, 20 μm. **B**, Representative photomicrographs TUNEL staining of LV sections from MI+PBS **(a)** and MI+αGC **(b)** and summary data for the number of TUNEL-positive cells in the noninfarcted LV (n=6). Scale bar, 20 μm. Data are expressed as mean±SEM. *P<0.05 versus sham+PBS, †P<0.05 versus MI+PBS.

CD11c (a marker of M1 macrophage) and arginase 1 (a marker of M2 macrophage) gene expressions were significantly increased in noninfarcted LV from MI+PBS compared with sham+PBS at day 7 (Figure 6A and 6B). αGC significantly increased their expressions in both sham and MI animals at day 7. Arginase 1 but not CD11c was increased in noninfarcted LV from MI+PBS and MI+αGC at day 28. There was no significant difference in arginase 1 between these 2 groups. MCP-1 and RANTES gene expressions were increased in noninfarcted LV from MI+PBS compared with sham+PBS at day 7 (Figure 6C and 6D). αGC significantly increased their expressions in both sham and MI animals at day 7. In contrast, there was no significant difference in their expressions among all groups at day 28.

IFN-γ, TNF-α, IL-6, and IL-10 gene expression levels were significantly increased in sham and MI mice by αGC at

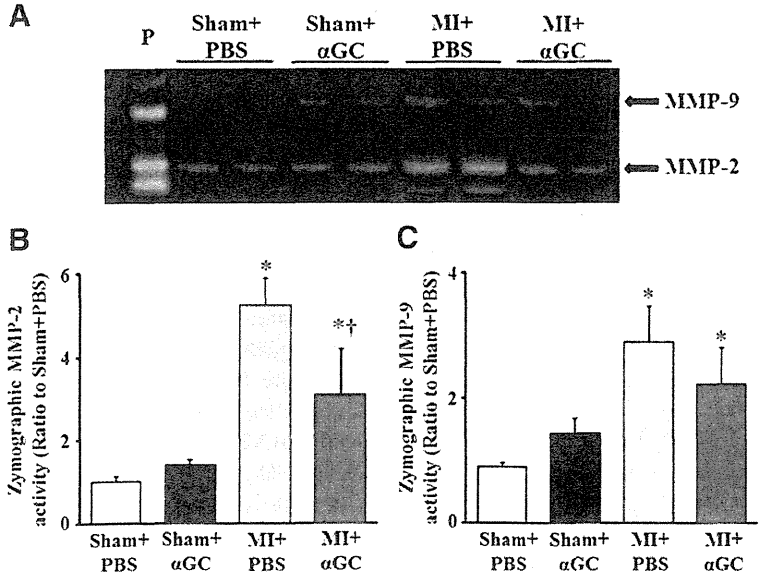

Figure 4. Representative LV zymographic MMP-2 and MMP-9 activities in noninfarcted LV at 7 days after surgery (A) and their densitometric analysis (B and C; n=5 for each). P indicates positive control. Data are expressed as mean±SEM. *P<0.05 versus sham+PBS, †P<0.05 versus MI+PBS.

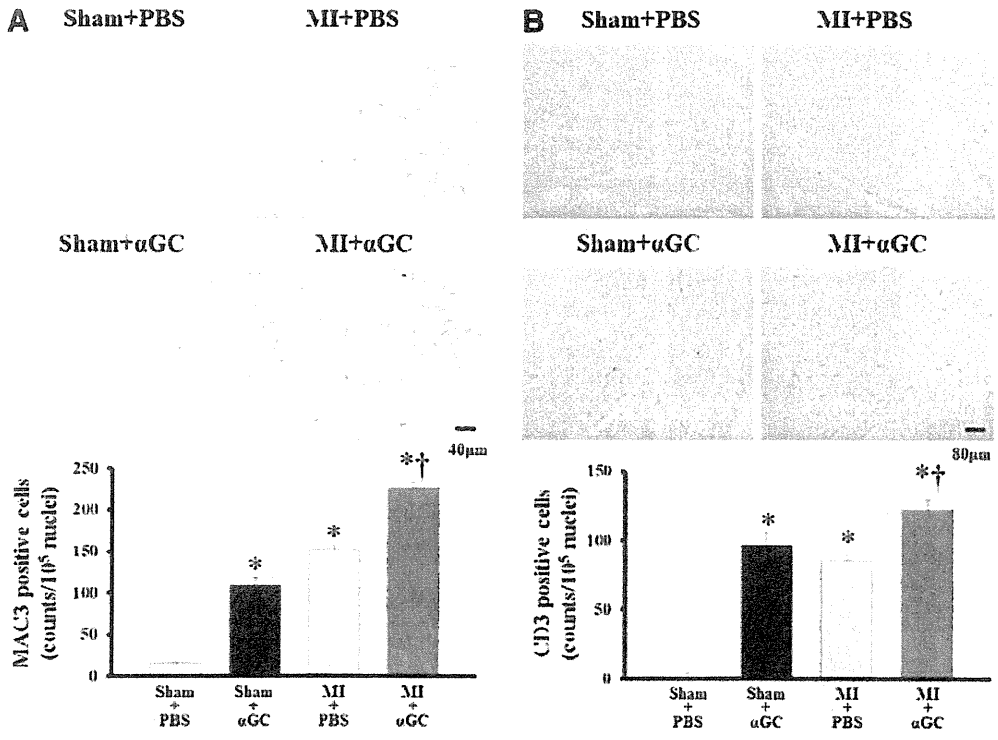

Figure 5. Representative photomicrographs of LV cross sections stained with (A, upper panel) anti-MAC3 and (B, upper panel), anti-CD3 in sham+PBS, sham+αGC, MI+PBS, and MI+αGC. Summary data of the numbers of **(A, lower panel)** MAC3 and **(B, lower panel)** CD3-positive cells in the LV (n=4–8 for each). Data are mean±SEM. *P<0.05 versus sham+PBS, †P<0.05 versus MI+PBS.

day 7 (Figure 6E through 6H). IL-10 gene expression alone significantly elevated up to 2.6-fold in the noninfarcted LV from MI+αGC mice at day 28 (Figure 6H). These time-dependent and αGC-mediated changes in IL-10 gene expression (Figure 6H) in the LV were matched with those in NKT cell infiltration (Figure 1B). IL-4 was not detected in either group.

Plasma Cytokine Concentration

Plasma IL-10 level was similar among sham+PBS, sham+αGC, and MI+PBS groups (9.0±0.5 versus 9.8±2.3 versus 10.6±2.3 pg/mL). However, in parallel to IL-10 gene expression in the LV, it significantly increased up to 2-fold in MI+αGC (21.1±2.3 pg/mL) compared with sham and MI+PBS mice (P<0.05). Plasma IFN-γ level was similar among 4 groups of mice (1.4±0.3 versus 1.7±0.3 versus 0.9±0.2 versus 1.0±0.2 pg/mL, P=NS). Plasma TNF-α, IL-6, and IL-4 levels were not detected in either group.

Experiment 3: Effects of IL-10 Neutralization on αGC-Treated Post-MI Heart Survival

The survival rate during 28 days tended to be higher in MI+αGC than in MI+anti–IL-10 receptor antibody and MI+αGC+anti–IL-10 receptor antibody (66.7% versus 44.4% and 42.1%, P=0.4).

Echocardiography and Hemodynamics

The echocardiographic and hemodynamic data from 3 groups of surviving mice are shown in Table 2. IL-10 receptor antibody injection significantly increased LV diameters, LVEDP, and decreased LV fractional shortening in αGC-treated MI mice. In contrast, there were no differences in these parameters between MI+anti–IL-10 receptor antibody and MI+αGC+anti–IL-10 receptor antibody. There was no significant difference in heart rate and aortic blood pressure among 3 groups.

Organ Weights and Infarct Size

In agreement with LVEDP, lung weight/body weight ratio was significantly increased in MI+αGC+anti–IL-10 receptor antibody compared with MI+αGC (Table 2). There were also no differences in these parameters between MI+anti–IL-10 receptor antibody and MI+αGC+anti–IL-10 receptor antibody.

Infarct size was comparable (56±2%, 54±2%, and 56±4%; P=NS) among MI+αGC (n=8), MI+anti–IL-10 antibody (n=8), and MI+αGC+anti–IL-10 receptor antibody (n=8) groups.

Experiment 4: Specificity of αGC for iNKT Cells

Immunohistochemical stainings for MAC3 and CD3 were increased in KO+MI+PBS compared with KO+sham+PBS. In contrast to the results from wild-type (Figure 5), αGC did not alter them (Online Figure I). MPO-positive cells were not detected in the LV tissue from either group of mice (data not shown). MCP-1 and RANTES were increased in KO+MI+PBS compared with KO+sham+PBS and were not affected by αGC (Online Figure IIA and B). There was

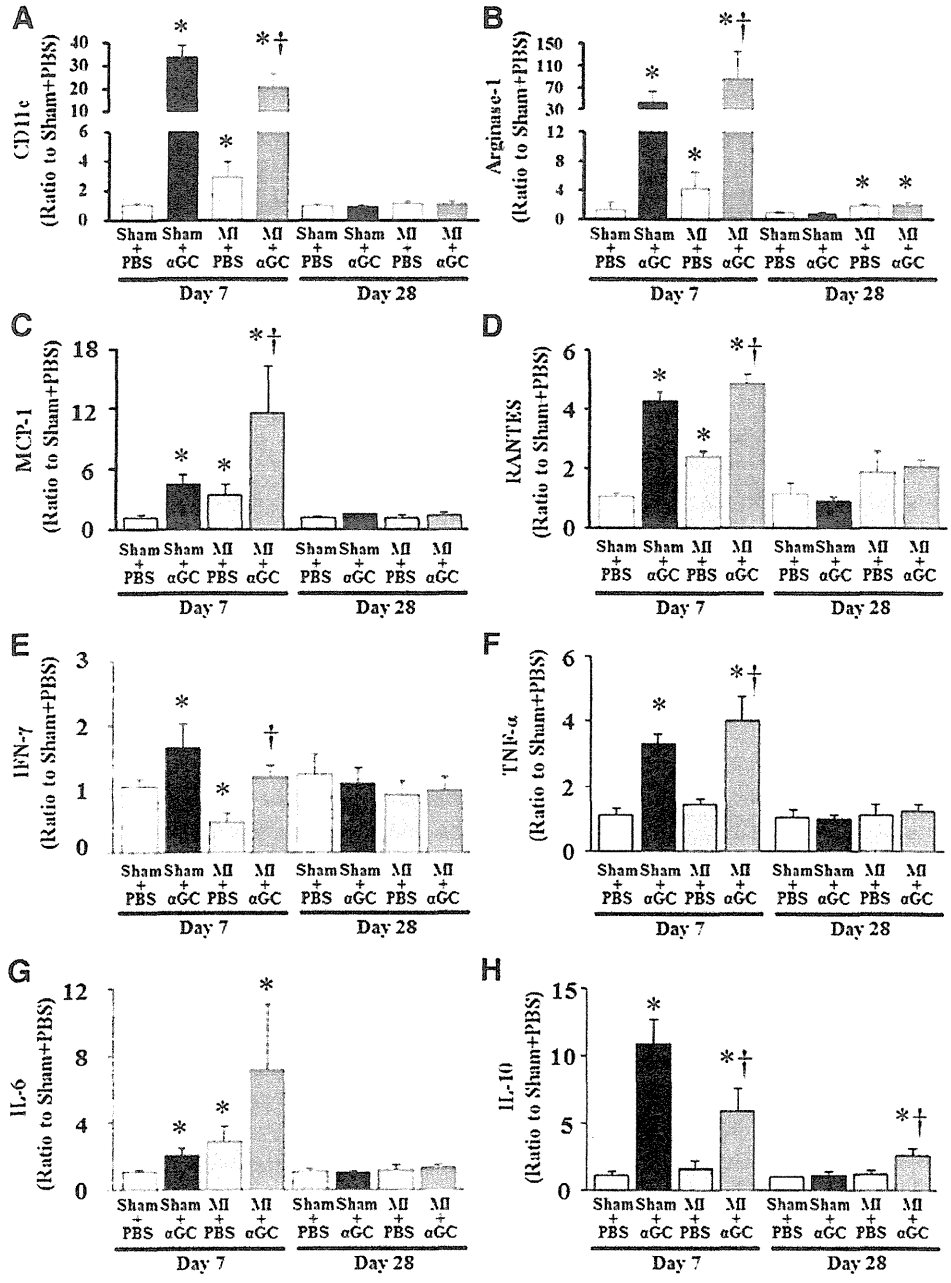

Figure 6. Quantitative analysis of gene expression of CD11c (A), arginase (B), MCP-1 (C), RANTES (D), IFN-γ (E), TNF-α (F), IL-6 (G), and IL-10 (H) in the noninfarcted LV at day 7 (n=6) and day 28 (n=4) after surgery. Gene expression was normalized to GAPDH and depicted as the ratio to sham+PBS. Data are expressed as mean±SEM. *$P<0.05$ versus sham+PBS, †$P<0.05$ versus MI+PBS.

no difference in TNF-α and IL-10 in the LV tissue from either group of mice (Online Figure IIC and D). These data suggest that αGC did not directly activate other inflammatory cell, induce chemokines, or produce inflammatory cytokines.

Discussion

The present study demonstrated that the activation of iNKT cells by αGC improved survival and ameliorated LV remodeling and failure after MI in mice, accompanied by the decreases in interstitial fibrosis, cardiomyocyte hypertrophy, and apoptosis. Furthermore, the enhanced expression of IL-10 by αGC is involved in these effects. This is the first report to provide direct evidence for increased iNKT cells in MI and the inhibitory effects of their activation on the development of post-MI HF.

Chronic Infiltration of Inflammatory Cells Including iNKT Cells in Post-MI Heart

In the setting of acute MI, the infiltration of inflammatory cells such as neutrophils, macrophages, and lymphocytes is a physiological repair process and beneficial removing dead cardiomyocytes and leading to the repair and scar formation of infarcted area.[18] However, the chronic inflammatory response in the noninfarcted area causes the further myocardial damage and fibrosis, leading to the progressive impairment of cardiac function.[19] We have previously demonstrated that anti–MCP-1 gene therapy improved survival and attenuated LV dilation and contractile dysfunction, which was associated with the decreases in macrophage infiltration and gene expression of myocardial inflammatory cytokines.[2] Therefore, chronic myocardial inflammation plays a crucial role on

Table 2. Echocardiography, Hemodynamics, and Organ Weights in Experiment 3

	MI+αGC (n=8)	MI+Anti–IL-10 Receptor Antibody (n=8)	MI+αGC+ Anti–IL-10 Receptor Antibody (n=8)
Echocardiography			
Heart rate, bpm	516±18	519±16	510±18
LVEDD, mm	4.8±0.1	5.4±0.1*	5.4±0.1*
LVESD, mm	3.9±0.1	4.6±0.1*	4.6±0.1*
FS, %	19±0.8	14.5±0.7*	15.4±0.7*
AWT, mm	0.30±0.01	0.37±0.06	0.35±0.06
PWT, mm	0.98±0.02	1.02±0.02	0.99±0.04
Hemodynamics			
Heart rate, min	518±16	487±17	515±22
Mean AoP, mm Hg	86±3	81±4	82±2
LVEDP, mm Hg	5.4±0.8	10.8±0.7*	11.4±3.3*
LV +dP/dt, mm Hg/s	10 441±661	6555±1031	7719±1284
LV –dP/dt, mm Hg/s	6847±569	4119±364	5774±1236
Organ weights			
Body wt, g	25.2±0.5	24.7±1.3	25.8±0.6
Heart wt/body wt, mg/g	6.3±0.3	8.8±0.9	6.9±0.5
Lung wt/body wt, mg/g	5.5±0.1	10.9±2.1*	7.9±1.0*
Infarct size, %	56±2	54±2	56±4

LVEDD indicates left ventricular end-diastolic diameter; LVESD, left ventricular end-systolic diameter; FS, fractional shortening; AWT, anterior wall thickness; PWT, posterior wall thickness; AoP, aortic pressure; LVEDP, left ventricular end-diastolic pressure; wt, weight. Data are mean±SEM.

*$P<0.05$ versus MI+ αGC.

LV remodeling and failure after MI. However, the precise role of various inflammatory cells and chemokines in this disease process has not been fully elucidated. iNKT cells are specialized lineage of T cells that recognize glycolipid antigens presented by the MHC class I–like molecule CD1d. The iNKT cells mediate various functions rapidly by producing a mixture of T_H1 and T_H2 cytokines and vast array of chemokines.[6] Thus, iNKT cells can function as a bridge between the innate and adaptive immune systems and orchestrate tissue inflammation. However, to our knowledge, there has been only one paper, by Olson et al, that reported the presence of iNKT cells in cardiac tissue obtained from acute Lyme carditis model.[20] Therefore, the present study was the first that demonstrated the increased infiltration of iNKT cells in post-MI hearts (Figure 1).

Effects of the Activation of iNKT Cells by αGC in Post-MI Heart

The most important finding of this study was that the activation of iNKT cells by αGC improved survival and attenuated LV remodeling and failure after MI (Figures 2 and 3 and Table 1). The beneficial effects of αGC were not attributable to its MI size-sparing effect, because the infarct size calculated as %LV circumference was comparable between MI+PBS and MI+αGC mice. Furthermore, its effects might not be attributable to those on hemodynamics, because blood pressure and heart rate were not altered (Table 1). αGC, a glycosphingolipid, is a well-known iNKT cell receptor ligand that can specifically activate iNKT cells.[13] It has been demonstrated that iNKT cells expand dramatically 2 to 3 days after in vivo treatment with αGC and return to the baseline level by approximately 9 days after treatment.[21,22] Moreover, the effects of iNKT cell stimulation may differ according to the timing of αGC administration. In the model of experimental autoimmune encephalomyelitis, early immunization with αGC protected against this disease, whereas later immunization potentiated it.[23] In the present study, αGC injection significantly enhanced iNKT cell infiltration (Figure 1) and could effectively ameliorate post-MI LV remodeling and failure (Figures 2 and 3).

Role of IL-10 in the Inhibitory Effects of iNKT Cell Activation by αGC

Another important finding of the present study was that the enhanced expression of IL-10 was involved in the inhibitory effects of iNKT cell activation against LV remodeling and failure (Table 2). These results are consistent with the previous findings that the therapeutic effects of αGC against T_H1-like autoimmune diseases include 2 mechanisms such as a shift from T_H1 toward a T_H2 pattern[9–11,23] and the induction of immunosuppressive cytokine IL-10.[9,11,12] The present study demonstrated that IL-10 was increased in noninfarcted LV from sham and MI animals in association with an increase in iNKT cells after the treatment with αGC at 7 days (Figure 6C and 6D). Interestingly, the enhanced expression of IL-10 gene by αGC persisted only in MI mice. These changes of IL-10 gene expression (Figure 6D) completely corresponded to those of iNKT cells (Figure 1B). Moreover, the inhibitory effects of αGC on LV remodeling and HF were reversed by anti–IL-10 receptor antibody and the treatment with only anti–IL-10 antibody of MI mice did not affect LV remodeling and HF (Table 2). Therefore, these data suggest that IL-10 is not associated with the development of LV remodeling and HF after MI without αGC, and IL-10 is involved in the beneficial effects of iNKT cell activation against post-MI remodeling and failure. These findings were consistent with a recent study by Krishnamurthy et al, in which LV dimension and function by echocardiography after MI did not differ between wild-type and IL-10–null mice.[24]

Possible Mechanisms of IL-10 for the Attenuation of LV Remodeling

IL-10 can inhibit the production of proinflammatory cytokines by macrophages and T_H1 cells[25,26] and directly promote the death of inflammatory cells.[27] Furthermore, beyond its suppressive effects on inflammatory gene synthesis, IL-10 also regulates extracellular matrix[28] and angiogenesis.[29] In the present study, the activation of iNKT cells by αGC decreased cardiac myocyte hypertrophy and apoptosis and inhibited interstitial fibrosis possibly through inhibiting the zymographic MMP-2 level in noninfarcted LV (Figure 4). MMP-2 is ubiquitously distributed in cardiac myocytes and fibroblasts and has been shown to play a crucial role in the

development of cardiac remodeling after MI.[30] Theoretically, an increase in MMP activity would result in a decrease in the MMP substrate, collagens, whereas an inhibition of MMP would result in an increase in collagens. However, our previous study showed that the selective disruption of the MMP-2 gene attenuated interstitial fibrosis after MI.[30] Therefore, the decrease in zymographic MMP-2 level by αGC might be involved in the attenuation of interstitial fibrosis in our model. On the other hand, MMP-9 is mainly expressed in infiltrating inflammatory cells such as neutrophils and T lymphocytes. A previous report showed that subcutaneous injection of recombinant IL-10 suppressed inflammation and attenuated LV remodeling after MI in mice by inhibiting fibrosis via suppression of HuR/MMP-9 and by enhancing capillary density through the activation of STAT3.[31] Moreover, the previous study by Burchfield et al showed that IL-10 from transplanted bone marrow mononuclear cells contributed to cardiac protection after MI in association with a decrease in T lymphocyte accumulation, reactive hypertrophy, and myocardial collagen deposition.[32] However, in the present study, zymographic MMP-9 level was not affected by αGC, which was consistent with the infiltration of lymphocyte observed by immunohistochemical staining for CD3 (Figure 5). We also measured the protein levels of HuR/MMP-9 or STAT3 in the noninfarcted LV. However, these protein levels were not affected by αGC (data not shown).

Role of Other Inflammatory Cells and Cytokines

In agreement with the increase in macrophage infiltration by αGC, MCP-1 gene expression was increased. αGC increased not only M1 macrophages but also M2 macrophages, which tune inflammatory responses and promote tissue repair.[33] Therefore, the increase in M2 macrophage might neutralize the effect of the increased M1 macrophage and MCP-1. The present study also showed that TNF-α was increased in noninfarcted LV from MI+αGC (Figure 6). TNF-α is a proinflammatory cytokine considered to be cardiotoxic and induce LV dysfunction.[34] However, in contrast, TNF-α has also protective effects during the maladaptive transition to HF.[35] Indeed, the treatment of patients with HF with either soluble TNF receptor (RENEWAL) or an anti-TNF antibody (ATTACH) could not show clinical benefits.[36,37] Therefore, the increase in TNF-α by αGC would not necessarily lead to the aggravation of LV remodeling.

Limitations

There are several limitations to be acknowledged in the present study. First, we could not directly demonstrate the location of iNKT cells by the immunohistochemical analysis using biotinylated CD1d dimer (BD Bioscience) with loading of αGC according to the previous report by Kamijyuku et al.[38] We tried the double immunohistochemical staining, using antibodies for anti–Armenian hamster TCR-β-PE (BD Bioscience) and anti-mouse NK 1.1-APC (BD Bioscience) according to the newly published paper.[39] Furthermore, we also performed in situ hybridization using digoxigenin-labeled DNA probes for mouse Vα14Jα18. Unfortunately, however, we could not detect iNKT cells in situ in the heart. Even though we defined iNKT cells within the heart by using the gene expression as well as the flow cytometric analysis, further studies are needed to overcome some technical difficulties of in situ detection and clarify this important issue. Second, the underlying mechanisms responsible for the activation of iNKT cells after MI remain to be established. To date, the endogenous ligand for iNKT cells has not been known. Based on our results using αGC, a glycosphingolipid, sphingolipid ceramide may be a crucial intermediate, since ceramide has been shown to be synthesized by long-chain fatty acids and actually increased in the heart after coronary microembolization.[40] Third, the source of IL-10 production after the stimulation of αGC remains to be determined. IL-10 has been shown to be produced by iNKT cells themselves on exogenous stimulation.[41] In addition, IL-10 can be expressed and secreted from macrophages activated by iNKT cells.[42,43] In the present study, the activation of iNKT cells by αGC injection increased the infiltration of macrophage in sham and MI mice at 7 days; however, there was no difference in it between MI+PBS and MI+αGC at 28 days (Figure 6). Therefore, the main source of IL-10 production at later phase of αGC injection would be the cells other than macrophages.

In conclusion, iNKT cells have a protective effect on LV remodeling and failure after MI via enhanced IL-10 expression. Therefore, therapies designed to activate iNKT cells may be beneficial against the development of post-MI heart failure.

Acknowledgments

We thank Kaoruko Kawai, Akiko Aita, and Miwako Fujii for excellent technical assistance.

Sources of Funding

This study was supported by grants from the Ministry of Education, Science, and Culture (17390223, 20590854, 20117004, 21390236) and Hokkaido Heart Association Grant for Research.

Disclosures

None.

References

1. Pfeffer MA, Braunwald E. Ventricular remodeling after myocardial infarction: experimental observations and clinical implications. *Circulation.* 1990;81:1161–1172.
2. Hayashidani S, Tsutsui H, Shiomi T, Ikeuchi M, Matsusaka H, Suematsu N, Wen J, Egashira K, Takeshita A. Anti-monocyte chemoattractant protein-1 gene therapy attenuates left ventricular remodeling and failure after experimental myocardial infarction. *Circulation.* 2003;108:2134–2140.
3. Varda-Bloom N, Leor J, Ohad DG, Hasin Y, Amar M, Fixler R, Battler A, Eldar M, Hasin D. Cytotoxic T lymphocytes are activated following myocardial infarction and can recognize and kill healthy myocytes in vitro. *J Mol Cell Cardiol.* 2000;32:2141–2149.
4. Shiomi T, Tsutsui H, Hayashidani S, Suematsu N, Ikeuchi M, Wen J, Ishibashi M, Kubota T, Egashira K, Takeshita A. Pioglitazone, a peroxisome proliferator-activated receptor-gamma agonist, attenuates left ventricular remodeling and failure after experimental myocardial infarction. *Circulation.* 2002;106:3126–3132.
5. Kaikita K, Hayasaki T, Okuma T, Kuziel WA, Ogawa H, Takeya M. Targeted deletion of CC chemokine receptor 2 attenuates left ventricular remodeling after experimental myocardial infarction. *Am J Pathol.* 2004;165:439–447.

6. Matsuda JL, Mallevaey T, Scott-Browne J, Gapin L. CD1d-restricted iNKT cells, the 'Swiss-Army knife' of the immune system. *Curr Opin Immunol.* 2008;20:358–368.
7. Nakai Y, Iwabuchi K, Fujii S, et al. Natural killer T cells accelerate atherogenesis in mice. *Blood.* 2004;104:2051–2059.
8. Ohmura K, Ishimori N, Ohmura Y, Tokuhara S, Nozawa A, Horii S, Andoh Y, Fujii S, Iwabuchi K, Onoe K, Tsutsui H. Natural killer T cells are involved in adipose tissues inflammation and glucose intolerance in diet-induced obese mice. *Arterioscler Thromb Vasc Biol.* 2010;30:193–199.
9. Hong S, Wilson MT, Serizawa I, Wu L, Singh N, Naidenko OV, Miura T, Haba T, Scherer DC, Wei J, Kronenberg M, Koezuka Y, Van Kaer L. The natural killer T-cell ligand alpha-galactosylceramide prevents autoimmune diabetes in non-obese diabetic mice. *Nat Med.* 2001;7:1052–1056.
10. Sharif S, Arreaza GA, Zucker P, et al. Activation of natural killer T cells by alpha-galactosylceramide treatment prevents the onset and recurrence of autoimmune Type 1 diabetes. *Nat Med.* 2001;7:1057–1062.
11. Furlan R, Bergami A, Cantarella D, Brambilla E, Taniguchi M, Dellabona P, Casorati G, Martino G. Activation of invariant NKT cells by alphaGalCer administration protects mice from MOG35–55-induced EAE: critical roles for administration route and IFN-gamma. *Eur J Immunol.* 2003;33:1830–1838.
12. Miellot A, Zhu R, Diem S, Boissier MC, Herbelin A, Bessis N. Activation of invariant NK T cells protects against experimental rheumatoid arthritis by an IL-10-dependent pathway. *Eur J Immunol.* 2005;35:3704–3713.
13. Van Kaer L. Alpha-galactosylceramide therapy for autoimmune diseases: prospects and obstacles. *Nat Rev Immunol.* 2005;5:31–42.
14. Kinugawa S, Tsutsui H, Hayashidani S, Ide T, Suematsu N, Satoh S, Utsumi H, Takeshita A. Treatment with dimethylthiourea prevents left ventricular remodeling and failure after experimental myocardial infarction in mice: role of oxidative stress. *Circ Res.* 2000;87:392–398.
15. Namba T, Tsutsui H, Tagawa H, Takahashi M, Saito K, Kozai T, Usui M, Imanaka-Yoshida K, Imaizumi T, Takeshita A. Regulation of fibrillar collagen gene expression and protein accumulation in volume-overloaded cardiac hypertrophy. *Circulation.* 1997;95:2448–2454.
16. Leuschner F, Panizzi P, Chico-Calero I, Lee WW, Ueno T, Cortez-Retamozo V, Waterman P, Gorbatov R, Marinelli B, Iwamoto Y, Chudnovskiy A, Figueiredo JL, Sosnovik DE, Pittet MJ, Swirski FK, Weissleder R, Nahrendorf M. Angiotensin-converting enzyme inhibition prevents the release of monocytes from their splenic reservoir in mice with myocardial infarction. *Circ Res.* 2010;107:1364–1373.
17. Kawano T, Cui J, Koezuka Y, Toura I, Kaneko Y, Motoki K, Ueno H, Nakagawa R, Sato H, Kondo E, Koseki H, Taniguchi M. CD1d-restricted and TCR-mediated activation of valpha14 NKT cells by glycosylceramides. *Science.* 1997;278:1626–1629.
18. Blankesteijn WM, Creemers E, Lutgens E, Cleutjens JP, Daemen MJ, Smits JF. Dynamics of cardiac wound healing following myocardial infarction: observations in genetically altered mice. *Acta Physiol Scand.* 2001;173:75–82.
19. Frangogiannis NG, Smith CW, Entman ML. The inflammatory response in myocardial infarction. *Cardiovasc Res.* 2002;53:31–47.
20. Olson CM Jr, Bates TC, Izadi H, Radolf JD, Huber SA, Boyson JE, Anguita J. Local production of IFN-gamma by invariant NKT cells modulates acute Lyme carditis. *J Immunol.* 2009;182:3728–3734.
21. Crowe NY, Uldrich AP, Kyparissoudis K, Hammond KJ, Hayakawa Y, Sidobre S, Keating R, Kronenberg M, Smyth MJ, Godfrey DI. Glycolipid antigen drives rapid expansion and sustained cytokine production by NK T cells. *J Immunol.* 2003;171:4020–4027.
22. Wilson MT, Johansson C, Olivares-Villagomez D, Singh AK, Stanic AK, Wang CR, Joyce S, Wick MJ, Van Kaer L. The response of natural killer T cells to glycolipid antigens is characterized by surface receptor down-modulation and expansion. *Proc Natl Acad Sci U S A.* 2003;100:10913–10918.
23. Jahng AW, Maricic I, Pedersen B, Burdin N, Naidenko O, Kronenberg M, Koezuka Y, Kumar V. Activation of natural killer T cells potentiates or prevents experimental autoimmune encephalomyelitis. *J Exp Med.* 2001;194:1789–1799.
24. Krishnamurthy P, Lambers E, Verma S, Thorne T, Qin G, Losordo DW, Kishore R. Myocardial knockdown of mRNA-stabilizing protein HuR attenuates post-MI inflammatory response and left ventricular dysfunction in IL-10-null mice. *FASEB J.*24:2484–2494.
25. Fiorentino DF, Zlotnik A, Vieira P, Mosmann TR, Howard M, Moore KW, O'Garra A. IL-10 acts on the antigen-presenting cell to inhibit cytokine production by Th1 cells. *J Immunol.* 1991;146:3444–3451.
26. Frangogiannis NG, Mendoza LH, Lindsey ML, Ballantyne CM, Michael LH, Smith CW, Entman ML. IL-10 is induced in the reperfused myocardium and may modulate the reaction to injury. *J Immunol.* 2000;165:2798–2808.
27. Wang P, Wu P, Siegel MI, Egan RW, Billah MM. Interleukin (IL)-10 inhibits nuclear factor kappa B (NF kappa B) activation in human monocytes. IL-10 and IL-4 suppress cytokine synthesis by different mechanisms. *J Biol Chem.* 1995;270:9558–9563.
28. Lacraz S, Nicod LP, Chicheportiche R, Welgus HG, Dayer JM. IL-10 inhibits metalloproteinase and stimulates TIMP-1 production in human mononuclear phagocytes. *J Clin Invest.* 1995;96:2304–2310.
29. Silvestre JS, Mallat Z, Duriez M, Tamarat R, Bureau MF, Scherman D, Duverger N, Branellec D, Tedgui A, Levy BI. Antiangiogenic effect of interleukin-10 in ischemia-induced angiogenesis in mice hindlimb. *Circ Res.* 2000;87:448–452.
30. Hayashidani S, Tsutsui H, Ikeuchi M, Shiomi T, Matsusaka H, Kubota T, Imanaka-Yoshida K, Itoh T, Takeshita A. Targeted deletion of MMP-2 attenuates early LV rupture and late remodeling after experimental myocardial infarction. *Am J Physiol Heart Circ Physiol.* 2003;285: H1229–H1235.
31. Krishnamurthy P, Rajasingh J, Lambers E, Qin G, Losordo DW, Kishore R. IL-10 inhibits inflammation and attenuates left ventricular remodeling after myocardial infarction via activation of STAT3 and suppression of HuR. *Circ Res.* 2009;104:e9–e18.
32. Burchfield JS, Iwasaki M, Koyanagi M, Urbich C, Rosenthal N, Zeiher AM, Dimmeler S. Interleukin-10 from transplanted bone marrow mononuclear cells contributes to cardiac protection after myocardial infarction. *Circ Res.* 2008;103:203–211.
33. Mantovani A, Sica A, Locati M. Macrophage polarization comes of age. *Immunity.* 2005;23:344–346.
34. Kubota T, McTiernan CF, Frye CS, Slawson SE, Lemster BH, Koretsky AP, Demetris AJ, Feldman AM. Dilated cardiomyopathy in transgenic mice with cardiac-specific overexpression of tumor necrosis factor-alpha. *Circ Res.* 1997;81:627–635.
35. Wang X, Oka T, Chow FL, Cooper SB, Odenbach J, Lopaschuk GD, Kassiri Z, Fernandez-Patron C. Tumor necrosis factor-alpha-converting enzyme is a key regulator of agonist-induced cardiac hypertrophy and fibrosis. *Hypertension.* 2009;54:575–582.
36. Mann DL, McMurray JJ, Packer M, et al. Targeted anticytokine therapy in patients with chronic heart failure: results of the Randomized Etanercept Worldwide Evaluation (RENEWAL). *Circulation.* 2004;109: 1594–1602.
37. Chung ES, Packer M, Lo KH, Fasanmade AA, Willerson JT. Randomized, double-blind, placebo-controlled, pilot trial of infliximab, a chimeric monoclonal antibody to tumor necrosis factor-alpha, in patients with moderate-to-severe heart failure: results of the anti-TNF Therapy Against Congestive Heart Failure (ATTACH) trial. *Circulation.* 2003;107: 3133–3140.
38. Kamijuku H, Nagata Y, Jiang X, et al. Mechanism of NKT cell activation by intranasal coadministration of alpha-galactosylceramide, which can induce cross-protection against influenza viruses. *Mucosal Immunol.* 2008;1:208–218.
39. Barral P, Sanchez-Nino MD, van Rooijen N, Cerundolo V, Batista FD. The location of splenic NKT cells favours their rapid activation by blood-borne antigen. *EMBO J.* 2012;31:2378–2390.
40. Thielmann M, Dorge H, Martin C, Belosjorow S, Schwanke U, van De Sand A, Konietzka I, Buchert A, Kruger A, Schulz R, Heusch G. Myocardial dysfunction with coronary microembolization: signal transduction through a sequence of nitric oxide, tumor necrosis factor-alpha, and sphingosine. *Circ Res.* 2002;90:807–813.
41. Sonoda KH, Faunce DE, Taniguchi M, Exley M, Balk S, Stein-Streilein J. NK T cell-derived IL-10 is essential for the differentiation of antigen-specific T regulatory cells in systemic tolerance. *J Immunol.* 2001;166:42–50.

42. Platzer C, Docke W, Volk H, Prosch S. Catecholamines trigger IL-10 release in acute systemic stress reaction by direct stimulation of its promoter/enhancer activity in monocytic cells. *J Neuroimmunol.* 2000;105:31–38.

43. Troidl C, Mollmann H, Nef H, Masseli F, Voss S, Szardien S, Willmer M, Rolf A, Rixe J, Troidl K, Kostin S, Hamm C, Elsasser A. Classically and alternatively activated macrophages contribute to tissue remodelling after myocardial infarction. *J Cell Mol Med.* 2009;13:3485–3496.

Novelty and Significance

What Is Known?

- Chronic tissue inflammation plays an important role in the development of left ventricular (LV) dysfunction and LV remodeling.
- Invariant natural killer T (iNKT) cells are a specialized lineage of T cells with NK marker. These cells produce a mixture of T_H1 and T_H2 cytokines and a vast array of chemokines to orchestrate tissue inflammation.
- iNKT cells play a protective role in experimental autoimmune and inflammatory diseases.

What New Information Does This Article Contribute?

- iNKT cells could be detected in normal heart, and their infiltration was increased in noninfarcted LV after myocardial infarction (MI).
- The activation of iNKT cells by α-galactosylceramide (αGC) improved survival and ameliorated LV remodeling and failure after MI in mice, accompanied by decreases in interstitial fibrosis, cardiomyocyte hypertrophy, and apoptosis.
- An increase in the expression of interleukin (IL)-10 by αGC was involved in the favorable effects for LV remodeling after MI.

iNKT cells regulate tissue inflammation by producing a mixture of T_H1 and T_H2 cytokines. Although chronic tissue inflammation is involved in the development of LV remodeling and failure, the pathophysiological role of iNKT cells in these processes have not been elucidated. Our study shows that infiltration of iNKT cells was increased in noninfarcted LV and their activation by αGC improved survival and ameliorated LV remodeling and failure after MI via enhanced expression of IL-10. These findings indicate a previously undescribed protective effect of iNKT cells on LV remodeling and failure after MI. Given that iNKT cells can bridge innate and adaptive immune systems, they could act as an upstream regulator of cytokine networks in the heart. Therapies designed to regulate iNKT cells and to modulate cytokine network may be beneficial in ameliorating LV remodeling and failure.

Supplemental Material

Detailed Methods

An expanded Methods section is available in the online Data Supplement at http://circres.ahajournals.org.

All procedures and animal care were approved by our institutional animal research committee and conformed to the animal care guideline for the Care and Use of Laboratory Animals in Hokkaido University Graduate School of Medicine.

Experiment 1: Time-dependent Changes of iNKT Cell Receptors in Post-MI Hearts

Animal Models

MI was created in male C57BL/6J mice, 6-8 weeks old and 20 to 25 g body weight, by ligating the left coronary artery as described previously.[1] Sham operation without ligating the coronary artery was also performed as control. MI mice were sacrificed and the hearts were excised at day 3, 7, 14 and 28 for quantitative reverse transcriptase (qRT)-PCR measurements.

Quantitative Reverse Transcriptase PCR

Total RNA was extracted from LV in sham mice and non-infarcted and infarcted LV from MI mice by using QuickGene-810 (FujiFilm, Tokyo, Japan) according to the manufacturer's instructions. cDNA was synthesized with the high capacity cDNA reverse transcription kit (Applied Biosystems, Foster City, CA). TaqMan quantitative PCR was performed with the 7300 real-time PCR system (Applied Biosystems) to amplify samples for Vα14Jα18 (a specific marker of iNKT cells).[2] This transcript was normalized to GAPDH. The primer was purchased from Applied Biosystems.

Experiment 2: Effects of iNKT Cell Activation on Post-MI Hearts

Animal Models

Sham and MI mice were created in male C57BL/6J as described in Experiment 1. Each group of mice was randomly divided into 2 groups; either α-galactosylceramide (αGC; 0.1μg/g body weight; Funakoshi Company, Ltd., Tokyo, Japan), the activator of iNKT cells, or phosphate-buffered saline (PBS) was administered via intraperitoneal injection 1 and 4 days after surgery. The concentration of αGC was chosen based on the previous study of its efficacy.[2] Thus, the experiment was performed in the following 4 groups of mice; sham+PBS (n=10), sham+αGC (n=10), MI+PBS (n=31), and MI+αGC (n=27).

Four weeks after surgery, echocardiographic studies and the hemodynamics measurement were performed. After collecting blood samples, mice were sacrificed and organ weight was measured. These measurements were performed in all survived mice (n=10 for sham+PBS, n=10 for sham+αGC, n=10 for MI+PBS, and n=16 for MI+αGC). The mice were further divided into 2 groups; for the histological analysis, including infarct size, myocyte cross-sectional area, collagen volume fraction, TUNEL staining (n=6 for each group), and for the quantitative reverse transcriptase PCR (n=4 for

each group). Additional mice were also created for MMP zymography (n=5 for each group) and for flow cytometry analysis (n=9 for each group).

A separate group of additional mice treated identically was created. One week after surgery, all mice (n=15 for each group) were sacrificed. These mice were used for immunohistochemistry (n=3 for each group), for the quantitative reverse transcriptase PCR (n=6 for each group), and for flow cytometry (n=9 for each group).

Survival

The survival analysis was performed in all 4 groups of mice. During the study period, the cages were inspected daily for deceased animals. All deceased mice were examined for the presence of MI as well as pleural effusion and cardiac rupture.

Echocardiographic and Hemodynamic Measurements

Echocardiographic and hemodynamic measurements were performed under light anesthesia with tribromoethanol/amylene hydrate (avertin; 2.5% wt/vol, 8 μL/g ip) with known short duration of action and modest cardiodepressive effects. A two-dimensional parasternal short-axis view was obtained at the levels of the papillary muscles. In general, the best views obtained with the transducer lightly applied to the mid upper left anterior chest wall. The transducer was then gently moved cephalad or caudad and angulated until desirable images were obtained. After it had been ensured that the imaging was on the axis, two-dimensional targeted M-mode tracings were recorded at a paper speed of 50mm/s. A 1.4-Fr micromanometer-tipped catheter (Millar Instruments, Houston, Texas) was inserted into the right carotid artery and then advanced into the left ventricle (LV) to measure LV pressures.

Myocardial Histopathology and Infarct Size

After mice were sacrificed, the heart was excised and dissected into right ventricle and LV including septum. LV was cut into three transverse sections; apex, middle ring, and base. From the middle ring, 5-μm sections were cut and stained with Masson's trichrome. Myocyte cross-sectional area and collagen volume fraction were determined by quantitative morphometry of tissue sections from the mid-LV as described previously.[3]

Infarct length was measured along the endocardial and epicardial surfaces in each of the cardiac sections, and the values from all specimens were summed. Infarct size (as a percentage) was calculated as total infarct circumference divided by total cardiac circumference.[1]

Myocardial Apoptosis

To detect apoptosis, tissue sections from the mid-LV were stained with the terminal deoxynucleotidyl transferase-mediated dUTP nick end-labeling (TUNEL) staining (TaKaRa Shuzo Co. Ltd., Ohtsu, Japan). The number of TUNEL positive cardiac myocyte nuclei was counted, and the data were normalized per 10^5 total nuclei identified by hematoxylin-positive staining in the same sections. The proportion of apoptotic cells was counted in the non-infarcted LV.

MMP Zymography

Zymographic MMP 2 and 9 levels in LV non-infarcted tissue was determined using gelatin zymography kit (Primary Cell Co., Ltd, Sapporo, Japan). The zymograms were digitized, and the size-fractionated bands, which indicated proteolytic levels, were measured by the integrated optical density in a rectangular region of interest.[1]

Isolation of Cardiac Mononuclear Cell and Flow Cytometry

LV tissue was harvested, minced with a fine scissors, placed in 10 ml RPMI-1640 with 5% FBS, 1 mg/ml collagenase type IV and 100 U/ml DNase I, and shaken at 37 °C for 45 min. Tissue was then triturated through nylon mesh and centrifuged (1400 rpm, 5min, 4 °C). Red blood cells were lysed with Tris-NH_4Cl solution. Cardiac mononuclear cells were isolated by density-gradient centrifugation with 33% Percoll™, as previously described.[4] Cardiac mononuclear cells from 3 mice were pooled, and subjected to flow cytometric analysis. All reagents were purchased from Sigma-Aldrich (St Louis, MO). Cardiac cell numbers were determined with Trypan blue (Wako Pure Chemical Industries, Ltd., Osaka, Japan).

The cells were incubated with 2.4G2 monoclonal antibody (mAb) to block non-specific binding of primary mAb and then reacted with Dimer X (CD1d:Ig recombinant fusion protein; BD Biosciences Pharmingen, San Diego, CA) loaded with αGC, followed by detection with phycoerythrin (PE)-conjugated anti-mouse IgG1 mAb (BD) according to the manufacturer's protocol.[5] After washing, cells were stained with a combination of fluorescein isothiocyanate (FITC)-anti-TCRβ and PE-anti-mouse IgG1 (all from BD Biosciences). Stained cells were acquired with FACS Canto II flow cytometer (BD Biosciences Immunocytometry Systems, San Jose, CA) and analyzed with FlowJo (Tommy Digital Biology, Tokyo, Japan). Propidium iodide (Sigma-Aldrich, St Louis, MO) positive cells were electronically gated as dead cells from the analysis.

RT-PCR

RNA was extracted and cDNA was synthesized were described in Experiment 1. TaqMan quantitative PCR was performed with the 7300 real-time PCR system (Applied Biosystems) to amplify samples for Vα14Jα18, CD11c (a marker of M1 macrophages), arginase-1 (a marker of M2 macrophages), MCP-1, RANTES, interferon-γ (IFN-γ), IL-4, IL-6, TNF-α, and IL-10 cDNA. These transcripts were normalized to GAPDH.

Immunohistochemistry

LV sections were immunostained with antibody against mouse MAC3 (a macrophage marker), mouse CD3 (a T cell marker), or mouse myeloperoxidase (a leucocyte marker), followed by counter-staining with hematoxylin.

Plasma Cytokines Concentration

Plasma IL-10, TNF-α, IFN-γ, IL-6, and IL-4 levels were measured by commercially

available ELISA kit (R&D systems, Inc.) in all groups.

Experiment 3: Effects of IL-10 Neutralization on αGC-Treated Post-MI Hearts

MI mice were divided into the following 3 groups of mice; MI+αGC (n=18), MI+anti-IL-10 receptor antibody (n=12), and MI+αGC+anti-IL-10 receptor antibody (n=19). αGC was administered identically as in Experiment 2. Anti-IL-10 receptor antibody (500μg/mouse, BD Pharmingen, San Diego, CA) was administered via intraperitoneal injection 1, 4, and 14 days after surgery. The concentration of anti-IL-10 receptor antibody was chosen based on the previous study of its efficacy.[6] Four weeks after surgery, echocardiographic and hemodynamics measurement were performed as described in Experiment 2. Separate set of mice from Experiment 2 was used in MI+αGC group.

Experiment 4: Specificity of αGC for NKT Cells

$V\alpha14^{+}$ NKT cell-deficient $J\alpha18^{-/-}$ (Jα18 KO) mice were provided from Dr. M. Taniguchi (RIKEN, Yokohama, Japan) and backcrossed 10 times to C57BL/6J.[7] Sham and MI mice were created in male Jα18 KO mice as described in Experiment 1. Each group of mice was treated identically to Experiment 2. Thus, the experiment was performed in the following 4 groups of mice; KO+sham+PBS, KO+sham+αGC, KO+MI+PBS, and KO+MI+αGC. One week after surgery, all mice (n=9 for each group) were sacrificed, and used for immunohistochemistry (n=3 for each group), and for the quantitative reverse transcriptase PCR (n=6 for each group). These analyses were performed as described in Experiment 2.

Statistical Analysis

Data were expressed as means ± SE. Survival analysis was performed by the Kaplan-Meier method, and between-group differences in survival were tested by the log-rank test. A between-group comparison of means was performed by 1-way ANOVA, followed by t test. The Bonferroni correction was applied for multiple comparisons of means. $P<0.05$ was considered statistically significant.

The authors had full access to and take full responsibility for the integrity of the data. All authors had read and agreed to the manuscript as written.

Supplemental Figures and Figure Legends

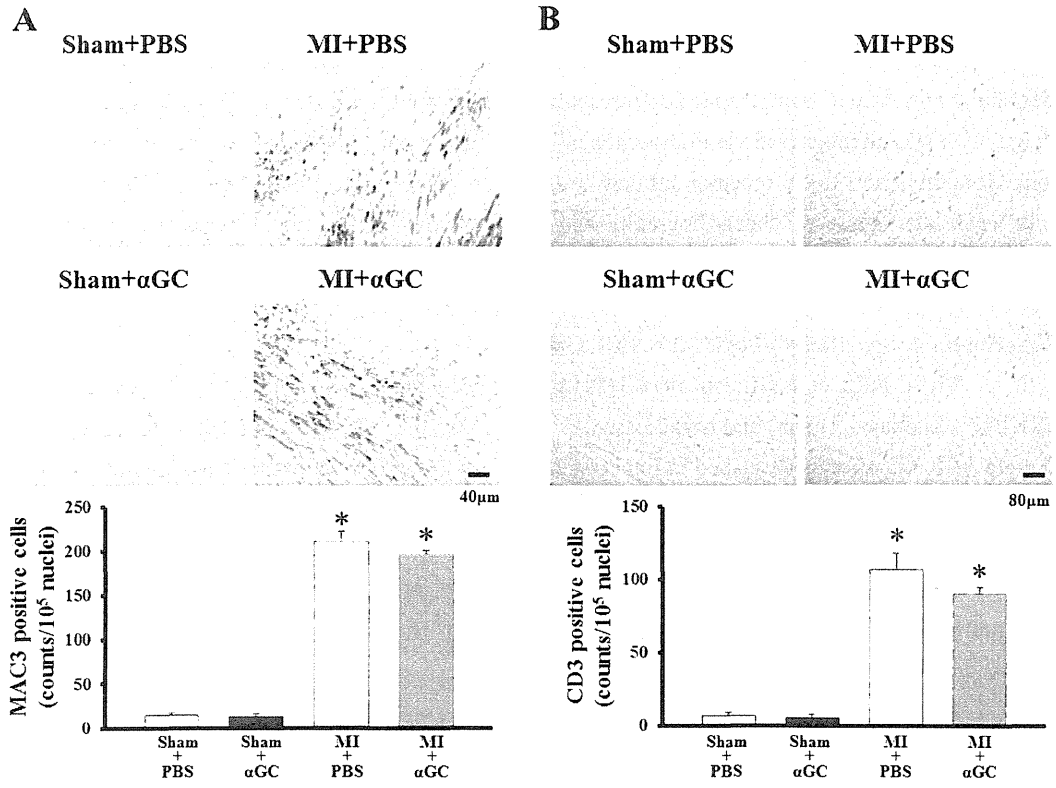

Online Figure I. Representative photomicrographs of LV cross-sections stained with (**A, upper panel**) anti MAC-3 and (**B, upper panel**) anti CD3 in KO+Sham+PBS, KO+Sham+αGC, KO+MI+PBS and KO+MI+αGC. Summary data of the numbers of (**A, lower panel**) MAC-3 and (**B, lower panel**) CD3 positive cells in the LV (n=4-8 for each). Data are means±SE. **P*<0.05 vs. Sham+PBS.

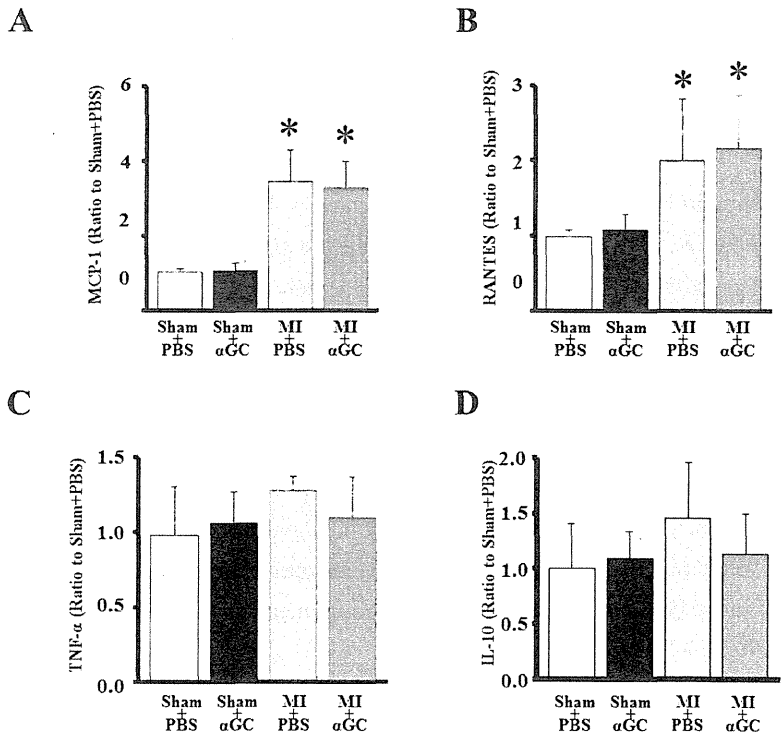

Online Figure II. Quantitative analysis of gene expression of MCP-1 (**A**), RANTES (**B**), TNF-α (**C**), and IL-10 (**D**) in the non-infarcted LV from KO mice at day 7 after surgery. Gene expression was normalized to GAPDH and depicted as the ratio to Sham+PBS. Data are expressed as means ± SE. **P*<0.05 vs. Sham+PBS.

Supplemental References

1. Kinugawa S, Tsutsui H, Hayashidani S, Ide T, Suematsu N, Satoh S, Utsumi H, Takeshita A. Treatment with dimethylthiourea prevents left ventricular remodeling and failure after experimental myocardial infarction in mice: role of oxidative stress. *Circ Res.* 2000;87:392-398.
2. Ohmura K, Ishimori N, Ohmura Y, Tokuhara S, Nozawa A, Horii S, Andoh Y, Fujii S, Iwabuchi K, Onoe K, Tsutsui H. Natural killer T cells are involved in adipose tissues inflammation and glucose intolerance in diet-induced obese mice. *Arterioscler Thromb Vasc Biol.* 2010;30:193-199.
3. Namba T, Tsutsui H, Tagawa H, Takahashi M, Saito K, Kozai T, Usui M, Imanaka-Yoshida K, Imaizumi T, Takeshita A. Regulation of fibrillar collagen gene expression and protein accumulation in volume-overloaded cardiac hypertrophy. *Circulation.* 1997;95:2448-2454.
4. Leuschner F, Panizzi P, Chico-Calero I, Lee WW, Ueno T, Cortez-Retamozo V, Waterman P, Gorbatov R, Marinelli B, Iwamoto Y, Chudnovskiy A, Figueiredo JL, Sosnovik DE, Pittet MJ, Swirski FK, Weissleder R, Nahrendorf M. Angiotensin-converting enzyme inhibition prevents the release of monocytes from their splenic reservoir in mice with myocardial infarction. *Circ Res.* 2010;107:1364-1373.
5. Nakai Y, Iwabuchi K, Fujii S, Ishimori N, Dashtsoodol N, Watano K, Mishima T, Iwabuchi C, Tanaka S, Bezbradica JS, Nakayama T, Taniguchi M, Miyake S, Yamamura T, Kitabatake A, Joyce S, Van Kaer L, Onoe K. Natural killer T cells accelerate atherogenesis in mice. *Blood.* 2004;104:2051-2059.
6. Miellot A, Zhu R, Diem S, Boissier MC, Herbelin A, Bessis N. Activation of invariant NK T cells protects against experimental rheumatoid arthritis by an IL-10-dependent pathway. *Eur J Immunol.* 2005;35:3704-3713.
7. Kawano T, Cui J, Koezuka Y, Toura I, Kaneko Y, Motoki K, Ueno H, Nakagawa R, Sato H, Kondo E, Koseki H, Taniguchi M. CD1d-restricted and TCR-mediated activation of valpha14 NKT cells by glycosylceramides. *Science.* 1997;278:1626-1629.

Arteriosclerosis, Thrombosis, and Vascular Biology

JOURNAL OF THE AMERICAN HEART ASSOCIATION

American Heart Association®

Interleukin-17A Deficiency Accelerates Unstable Atherosclerotic Plaque Formation in Apolipoprotein E-Deficient Mice

Keiko Danzaki, Yutaka Matsui, Masahiro Ikesue, Daichi Ohta, Koyu Ito, Masashi Kanayama, Daisuke Kurotaki, Junko Morimoto, Yoichiro Iwakura, Hideo Yagita, Hiroyuki Tsutsui and Toshimitsu Uede

Arterioscler Thromb Vasc Biol. 2012;32:273-280; originally published online November 23, 2011;
doi: 10.1161/ATVBAHA.111.229997
Arteriosclerosis, Thrombosis, and Vascular Biology is published by the American Heart Association, 7272 Greenville Avenue, Dallas, TX 75231

Print ISSN: 1079-5642. Online ISSN: 1524-4636

Interleukin-17A Deficiency Accelerates Unstable Atherosclerotic Plaque Formation in Apolipoprotein E-Deficient Mice

Keiko Danzaki, Yutaka Matsui, Masahiro Ikesue, Daichi Ohta, Koyu Ito, Masashi Kanayama, Daisuke Kurotaki, Junko Morimoto, Yoichiro Iwakura, Hideo Yagita, Hiroyuki Tsutsui, Toshimitsu Uede

Objective—Interleukin(IL)-17A, an inflammatory cytokine, has been implicated in atherosclerosis, in which inflammatory cells within atherosclerotic plaques express IL-17A. However, its role in the development of atheroscelrosis remains to be controversial.

Methods and Results—To directly examine the role of IL-17A in atherosclerosis, we generated apolipoprotein E (ApoE)/IL-17A double-deficient ($ApoE^{-/-}IL\text{-}17A^{-/-}$) mice. Mice were fed with high-fat diet (HFD) for either 8 or 16 weeks, both starting at ages of 6 to 8 weeks. We found that splenic $CD4^+$ T-cells produced high amounts of IL-17A in $ApoE^{-/-}$ mice after HFD feeding for 8 weeks. Atherosclerosis was significantly accelerated in HFD-fed $ApoE^{-/-}IL\text{-}17A^{-/-}$ mice compared with $ApoE^{-/-}$ mice. Splenic $CD4^+$ T-cells of $ApoE^{-/-}IL\text{-}17A^{-/-}$ mice after HFD feeding for 8 weeks, but not for 16 weeks, exhibited increased interferon gamma and decreased IL-5 production. Importantly, formation of vulnerable plaque as evidenced by reduced numbers of vascular smooth muscle cells and reduced type I collagen deposition in the plaque was detected in $ApoE^{-/-}IL\text{-}17A^{-/-}$ mice after HFD feeding for 8 weeks.

Conclusion—These results suggest that IL-17A regulates the early phase of atherosclerosis development after HFD feeding and plaque stability, at least partly if not all by modulating interferon gamma and IL-5 production from $CD4^+$ T-cells. (***Arterioscler Thromb Vasc Biol.* 2012;32:273-280.**)

Key Words: atherosclerosis ■ CD4 positive T cells ■ high fat diet ■ interferon gamma ■ interleukin-17A

Atherosclerosis is characterized by chronic inflammation of vessel walls and is initiated by infiltration of monocytes and activated T-cells into activated endothelium, followed by their migration into the intima and subsequent lipid accumulation within macrophages. Soluble mediators, such as inflammatory cytokines, produced by activated T-cells also affect the development of atherosclerosis.[1] $CD4^+$ T-cells are the predominant T-cell subset in atherosclerotic lesions in apolipoprotein E-deficient ($ApoE^{-/-}$) and LDL receptor-deficient ($LDLR^{-/-}$) mice.[2] On activation, $CD4^+$ T-cells differentiate into different T helper (Th) cell subsets with different cytokine profiles and distinct effector functions.[3] Historically, $CD4^+$ T-cells have been divided into Th1 and Th2 cells on the basis of the cytokines they produce. A third subset of interleukin (IL)-17A–producing $CD4^+$ T, called Th17 cells, has been discovered.[4] Murine IL-17A is a 21-kDa glycoprotein[5] that is produced not only by $CD4^+$ T-cells, but also by $CD8^+$ T-cells, γδ T-cells, neutrophils, and monocytes.[6] IL-17A induces the production of cytokines (eg, IL-6, granulocyte colony-stimulating factor, and granulocyte-macrophage colony-stimulating factor), chemokines (eg, CXCL1, CXCL5, IL-8, CCL2, and CCL7), and matrix metalloproteinases (eg, MMP-1, MMP-3, and MMP-13) from fibroblasts, endothelial cells, and epithelial cells. This suggests that IL-17A plays an important role in inflammatory processes.[6] In addition, Th17 cells play a central role in the development of autoimmune diseases, such as experimental autoimmune encephalomyelitis and collagen-induced arthritis, which have been previously believed to be Th1 cell-mediated diseases.[7,8]

With regard to atherosclerosis, several previous papers reported the critical role of interferon gamma (IFN-γ). IFN-γ expression has been detected within human atherosclerotic lesions[9] and IFN-γ–deficient mice exhibit attenuated atherosclerosis, whereas injections of recombinant IFN-γ increase

Received on: April 25, 2011; final version accepted on: November 9, 2011.

From the Division of Molecular Immunology (K.D., M.I., D.O., K.I., M.K., J.M., T.U.), Department of Matrix Medicine (Y.M., D.K., T.U.), Institute for Genetic Medicine, Hokkaido University, Sapporo, Japan; Center for Experimental Medicine and Systems Biology (Y.I.), Institute of Medical Science, University of Tokyo, Tokyo, Japan; Department of Immunology (H.Y.), Juntendo University, Tokyo, Japan; Department of Cardiovascular Medicine (H.T.), Hokkaido University Graduate School of Medicine, Sapporo, Japan.

Keiko Danzaki and Yutaka Matsui contributed equally to this study.

Correspondence to Toshimitsu Uede, MD, PhD, Division of Molecular Immunology, Institute for Genetic Medicine, Hokkaido University, Kita-15, Nishi-7, Kita-ku, Sapporo, 060-0815, Japan. E-mail toshi@igm.hokudai.ac.jp

Arterioscler Thromb Vasc Biol **is available at http://atvb.ahajournals.org** **DOI: 10.1161/ATVBAHA.111.229997**

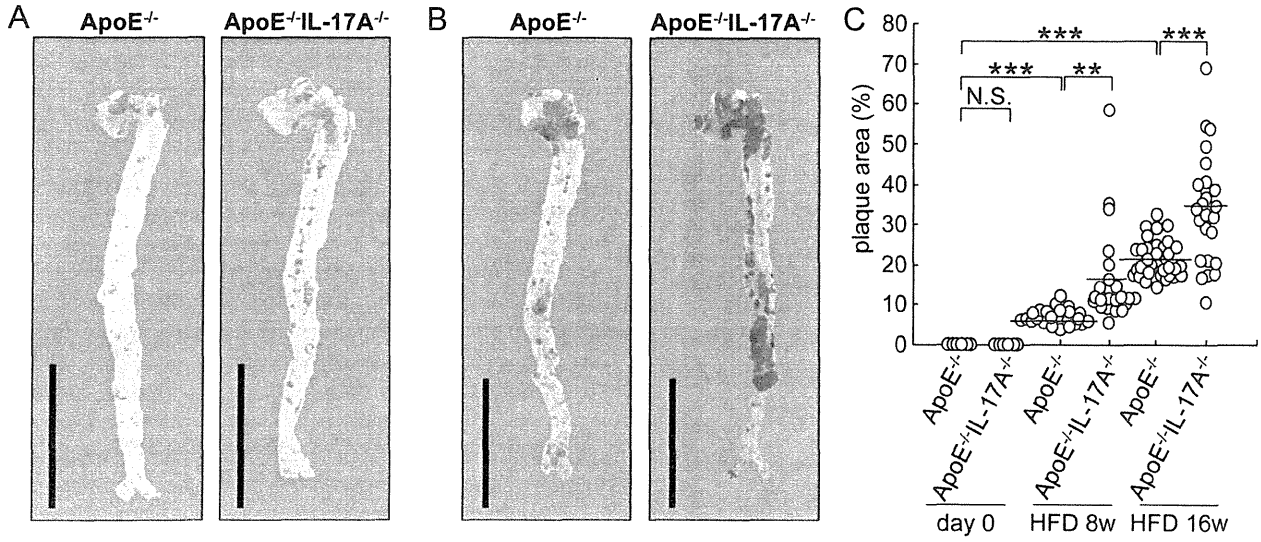

Figure 1. Interleukin (IL)-17A deficiency accelerates atherosclerotic plaque formation in apolipoprotein E (ApoE) double-deficient ($ApoE^{-/-}$) mice. Representative macroscopic image of aortae stained with oil red O in $ApoE^{-/-}$ and $ApoE^{-/-}IL\text{-}17A^{-/-}$ mice 8 weeks (**A**) and 16 weeks (**B**) after high-fat diet (HFD) feeding. Scale bars indicate 10 mm. **C**, Quantitative analysis of oil red O-stained aortae. Horizontal bars indicate mean values. $ApoE^{-/-}$: day 0 (n=5), 8 weeks (8w; n=23), 16 weeks (16w; n=34), $ApoE^{-/-}IL\text{-}17A^{-/-}$: day 0 (n=5), 8 weeks (n=22), and 16 weeks (n=24). $^{**}P<0.005$. $^{***}P<0.0005$. N.S., not significantly different.

lesion size.[10,11] Furthermore, Eid et al reported the presence of both IL-17A and IFN-γ in clinical specimens of coronary atherosclerosis and the presence of IL-17A/IFN-γ dual-producing T-cells within coronary plaques.[12] However, recent studies using atherosclerotic mouse models have indicated the crucial but controversial role of IL-17A in the progression of atherosclerosis. Some researchers suggest that IL-17A promotes atherosclerotic plaque formation,[13–17] or inhibition of IL-17A signaling does not alter lesion development in Th1-biased C57BL/6 $ApoE^{-/-}$ and $LDLR^{-/-}$ mice with already low levels of IL-17A production,[18] whereas others suggest that IL-17A suppresses the development of atherosclerosis.[19,20] Because it is still not clear why these studies found contradictory experimental results, we addressed whether IL-17A plays a role in atherosclerosis by using mice that completely lack IL-17A (IL-17A–deficient [$IL\text{-}17A^{-/-}$] mice) by crossing them with ApoE-deficient mice, which is the most common mice model for human atherosclerotic disease.[21,22] In this study, we determined whether and how IL-17A deficiency affects atherosclerotic plaque formation and discussed how our data can be incorporated into the previous controversial roles of IL-17A on atherosclerosis formation. It has been shown that premenopausal women have a significantly lower risk of developing atherosclerosis than age-matched men[23] and estrogen has antiatherogenic role in animal models.[24] Therefore, we focused on male mice.

Materials and Methods

Expanded materials and methods are available in the Supplemental Data, available online at http://atvb.ahajournals.org.

Mice and Induction of Atherosclerosis

All animal protocols were approved by the committee on animal experimentation of Hokkaido University. IL-17A–deficient mice used in this study were created as described previously.[25] C57BL/6 ApoE-deficient male mice ($ApoE^{-/-}$) (backcrossed 10 times; Jackson Laboratory, Bar Harbor, ME) were bred with IL-17A–deficient ($IL\text{-}17A^{-/-}$) female mice on a C57BL/6 background (backcrossed 10 times). IL-17A wild-type and IL-17A–deficient mice among ApoE-deficient mice were designated as $ApoE^{-/-}$ and $ApoE^{-/-}IL\text{-}17A^{-/-}$, respectively. Male $ApoE^{-/-}$ and $ApoE^{-/-}IL\text{-}17A^{-/-}$ mice were weaned at 6 to 8 weeks of age and fed an atherogenic high-fat diet (HFD) (0.15% cholesterol and 21% milk fat, 57BD; TestDiet, Richmond, IN) ad libitum for 8 or 16 weeks. Other $ApoE^{-/-}$ mice at ages of 6 to 8 weeks were fed with HFD for 12 weeks in the absence or presence of recombinant mouse IL-17 (eBioscience) (2 μg/mouse, twice per week).

Statistical Analysis

Results are expressed as mean (SEM). Statistical significance between groups was estimated using Student *t* test; $P<0.05$ was considered statistically significant.

Results

IL-17A Deficiency Accelerated Atherosclerotic Plaque Formation in $ApoE^{-/-}$ Mice

Starting at ages of 6 or 8 weeks, male $ApoE^{-/-}$ and $ApoE^{-/-}IL\text{-}17A^{-/-}$ mice were fed with HFD for 8 or 16 weeks and analyzed at ages of 14 to 16 or 22 to 24 weeks. Mean body weight was not significantly different between $ApoE^{-/-}$ and $ApoE^{-/-}IL\text{-}17A^{-/-}$ mice before and after HFD feeding (body weight before diet, $ApoE^{-/-}$=20.2±0.2 g, $ApoE^{-/-}IL\text{-}17A^{-/-}$=20.1±0.2 g, 8 weeks after diet; $ApoE^{-/-}$=27.7±0.7 g, $ApoE^{-/-}IL\text{-}17A^{-/-}$=29.6±0.9 g, 16 weeks after diet; $ApoE^{-/-}$=31.4±0.7 g, $ApoE^{-/-}IL\text{-}17A^{-/-}$=33.2±0.6 g). The development of atherosclerosis in the entire aorta was carefully analyzed. Representative macroscopic findings in $ApoE^{-/-}$ and $ApoE^{-/-}IL\text{-}17A^{-/-}$ mice are shown in Figure 1; the acceleration of lesion formation (red-stained areas) is evident in $ApoE^{-/-}IL\text{-}17A^{-/-}$ mice compared with $ApoE^{-/-}$ mice at 8 or 16 weeks after HFD feeding (Figure 1A and 1B, respectively). Individual data points are plotted by genotype in Figure 1C.

Before HFD feeding, there was no obvious plaque formation in both $ApoE^{-/-}$ and $ApoE^{-/-}IL\text{-}17A^{-/-}$ mice at ages

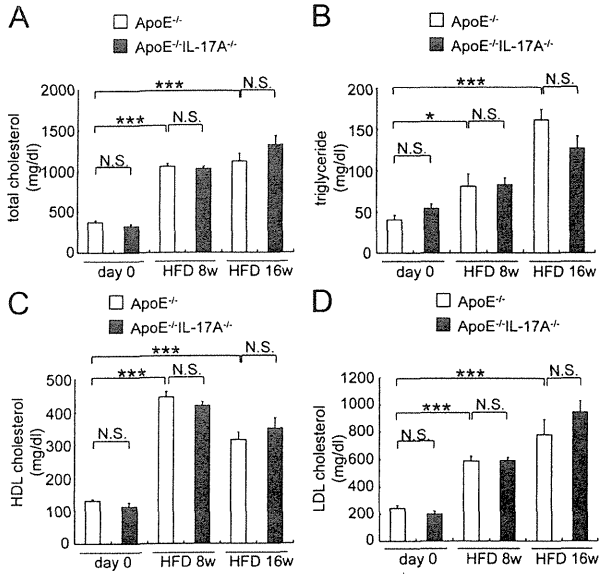

Figure 2. Interleukin (IL)-17A deficiency did not significantly affect lipid metabolism in apolipoprotein E (ApoE) double-deficient ($ApoE^{-/-}$) mice. To determine the effect of IL-17A deficiency on the level of serum cholesterol, we determined the concentrations of total cholesterol (**A**), triglycerides (**B**), HDL cholesterol (**C**), and LDL cholesterol (**D**) in $ApoE^{-/-}$ and $ApoE^{-/-}IL\text{-}17A^{-/-}$ mice before (day 0) and after HFD feeding (8 or 16 weeks). Day 0 and 8-week $ApoE^{-/-}$ (n=13), day 0 and 8-week $ApoE^{-/-}IL\text{-}17A^{-/-}$ (n=16), 16-week $ApoE^{-/-}$ (n=16–19), 16-week $ApoE^{-/-}IL\text{-}17A^{-/-}$ (n=18–22). Open bars indicate $ApoE^{-/-}$ mice. Closed bars indicate $ApoE^{-/-}IL\text{-}17A^{-/-}$ mice. $^{*}P<0.05$. $^{***}P<0.0005$. N.S., not significantly different.

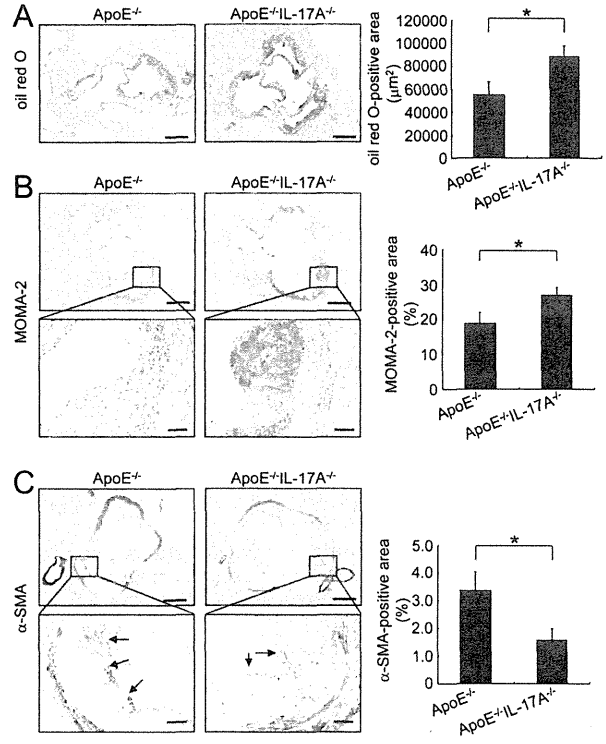

Figure 3. Effect of interleukin (IL)-17A deficiency on the nature of atherosclerotic plaque in aortic root sections in apolipoprotein E (ApoE) double-deficient ($ApoE^{-/-}$) mice. **A**, Representative microphotographs of aortic root sections stained with oil red O in $ApoE^{-/-}$ (n=11) and $ApoE^{-/-}IL\text{-}17A^{-/-}$ (n=16) mice after 8 weeks of high-fat diet (HFD) feeding. Red-stained areas indicate lipid-rich plaque. Scale bars indicate 300 μm. Quantitative analysis of data were shown in right panel. **B**, Representative microphotographs of the aortic root sections stained with MOMA-2 in $ApoE^{-/-}$ (n=11) and $ApoE^{-/-}IL\text{-}17A^{-/-}$ (n=15) mice after 8 weeks of HFD feeding. Scale bars in upper panels indicate 300 μm and in lower panels indicate 50 μm. **C**, Representative microphotographs of aortic root sections stained with α-smooth muscle actin (SMA) in $ApoE^{-/-}$ (n=11) and $ApoE^{-/-}IL\text{-}17A^{-/-}$ (n=16) mice after 8 weeks of HFD feeding. Arrows indicate α-SMA positive areas. Scale bars in upper panels indicate 300 μm and in under panels indicate 50 μm. **A**, **B**, and **C** sections were counterstained with hematoxylin. Statistical evaluation of data shown in **A**, **B**, and **C** were shown in right panels. $^{*}P<0.05$.

of 6 or 8 weeks (Figure 1C, day 0). Importantly, however, $ApoE^{-/-}IL\text{-}17A^{-/-}$ mice had significantly larger atherosclerotic lesions than $ApoE^{-/-}$ mice at both 8 and 16 weeks after HFD feeding, demonstrating that complete absence of IL-17A in atherogenic prone mice, $ApoE^{-/-}$ further promotes the development of HFD-induced atherosclerosis. It should be noted that there was a tendency of slight increase of plaque area in $ApoE^{-/-}IL\text{-}17A^{-/-}$ mice compared with $ApoE^{-/-}$ mice at 16 weeks after normal chow diet feeding, however, there was no statistically significant difference between 2 groups (Supplemental Figure I).

IL-17A Deficiency Did Not Significantly Affect Lipid Metabolism in $ApoE^{-/-}$ and $ApoE^{-/-}IL\text{-}17A^{-/-}$ Mice

Lipid metabolism critically influences the complex processes of atherosclerosis.[26,27] Total-, HDL-, and LDL-cholesterol and triglycerides levels were determined in $ApoE^{-/-}$ and $ApoE^{-/-}IL\text{-}17A^{-/-}$ mice before as well as at both 8 and 16 weeks after HFD feeding, to examine whether any of these factors were altered by the IL-17A genotype. Although the HFD significantly increased all cholesterol and triglycerides levels in $ApoE^{-/-}$ and $ApoE^{-/-}IL\text{-}17A^{-/-}$ mice, the IL-17A genotype had no significant effect on any cholesterol and triglycerides levels in $ApoE^{-/-}$ mice before and even after HFD feeding (Figure 2). These data indicate that the exacerbation in atherosclerotic lesions observed in $ApoE^{-/-}IL\text{-}17A^{-/-}$ mice is not attributable to the alterations in serum lipid metabolism.

Effect of IL-17A Deficiency on the Nature of Atherosclerotic Plaque in the Aortic Sections of $ApoE^{-/-}$ Mice

To determine how IL-17A affects the nature of plaques, we investigated atherosclerotic plaques in the aortic root sections of mice fed with HFD for 8 weeks. Consistent with the data from en face method (Figure 1), we found that IL-17A deficiency enhanced atherosclerotic plaque formation as defined by oil red O staining, in the aortic root sections of $ApoE^{-/-}$ mice (Figure 3A). We also found that in not only aortic roots, but also abdominal aorta, atherosclerosis was prominent in $ApoE^{-/-}IL\text{-}17A^{-/-}$ mice at 8 weeks after HFD feeding (Supplemental Figure II). In addition, MOMA-2–positive macrophage infiltration was greater in $ApoE^{-/-}IL\text{-}17A^{-/-}$ mice than $ApoE^{-/-}$ mice (Figure 3B). More importantly, the α-smooth muscle actin $(SMA)^{+}$ vascular smooth muscle cell (VSMC) number was significantly reduced at fibrous cap in $ApoE^{-/-}IL\text{-}17A^{-/-}$ mice